A Kalman Filter for Odometry using a Wheel Mounted Inertial Sensor

Bernd Gersdorf and Udo Frese
Cyber-Physical Systems, German Research Center for Artificial Intelligence, Bremen, Germany
{*bernd.gersdorf, udo.frese*}*@dfki.de*

Keywords: Extended Kalman Filter (EKF), Odometry, Wheel, Sensor, Inertial Measurement Unit (IMU), MEMS, Gyroscope, Accelerometer, Walker, Wheelchair, Tricycle, Navigation, ASSAM.

Abstract: This paper describes an Extended Kalman Filter for a wheel mounted inertial measurement unit using two accelerometers and a single gyroscope as a substitute for classical odometry sensing. The sensor can be mounted with minimal effort on existing wheeled vehicles. It is highly robust against vibration while rolling on uneven terrain and can cope with higher speeds even when the measurement range is partially exceeded. It has been developed as a component of a GPS based urban navigation assistant for elderly people using walkers, wheelchairs, or tricycles as an add-on device.

1 INTRODUCTION

Odometry is frequently used on wheeled robots as a measurement of travelled distance. Incremental encoders are attached near the wheel or in the motor to measure discrete angle steps interpreted as travelled distance. Integrating such a sensor is easy when considered in the mechanical design from the beginning, but adding an odometry sensor later on is often difficult. This is particular true for the application that motivates our research, where COTS (Commercial Off-The-Shelf) wheelchairs or walkers shall be equipped with odometry to give navigation support for elderly people. An alternative is a sensor attached at an arbitrary position on the wheel, that measures gravity to derive a wheel angle. Accelerometer based sensors are described by (Sonenblum, 2010) and (Huang and Wang, 2011), both using cheap MEMS sensors on tiny battery powered microcontroller boards for logging or wireless communication (details in Section 2).

A conceptual problem of an accelerometer based approach is its sensibility to vehicle acceleration and noise produced while driving over uneven terrain. As a solution, we propose an Extended Kalman Filter (Welch and Bishop, 1995), (Kalman, 1960), as a principled estimator for locally linear systems observed by noisy sensors. Given a proper process model accounting for all aspects of the kinematics for a wheel with its attached sensor, this filter can produce high quality estimates for (in this case) the wheel angle and, indirectly, the travelled distance. Angle accuracy at low speed or while standing using MEMS accelerometers is typically much better than required for the application area, but it is unacceptable to loose complete wheel revolutions under stress like uneven terrain or acceleration (e.g. while braking hard), especially when using odometry on both wheels of the same axis to derive the heading of the vehicle (details in Sections 5.1 and 5.2).

An alternative to a gravity sensor is a magnetic field sensor, frequently used as a low cost solution for bicycle computers to count wheel revolutions to derive speed and distance. Section 5.4 uses this technique as a reference measurement in the evaluation of the filter given in Section 4. In contrast to a gravity sensor, magnet sensor placement can be problematic, if the wheel hub contains a lot of iron.

This work was motivated by the ASSAM project (Krieg-Brückner et al., 2012), (Krieg-Brückner et al., 2013), that develops a navigation assistant for elderly people using COTS walkers, hand pushed wheelchairs, electric wheelchairs, and tricycles. The navigation assistance uses GPS as the main outdoor localization sensor supported at least by odometry for dead reckoning while in urban canyons, where the GPS signal is hidden or reflected by obstacles. In addition, it uses OSM (OpenStreetMap, 2013) card material enriched with sidewalks, stairs, and bicycle paths to provide more detailed and precise positions.

The wheel attached sensor shall finally communicate with a smart phone or tablet computer attached to the vehicle using Bluetooth® LE (Bluetooth, 2013), an upcoming standard for low energy wireless communication on hand held devices.

The remainder of this paper is structured as follows. Section 2 gives an overview of related work. The sensor hardware used for experiments is described in Section 3. Section 4 introduces the new Extended Kalman Filter, and Section 5 presents the filter in operation using real hardware as described in Section 3. We conclude in Section 6.

2 RELATED WORK

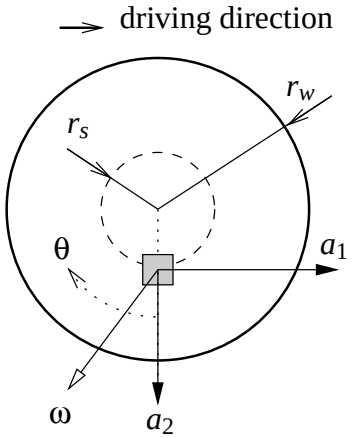

Figure 1: Sensor position for wheel angle θ=0 (grows positive in driving direction). Angular acceleration is measured by a_1, centrifugal force by a_2, and the gyroscope measures angular wheel speed ω.

An early reference to a sensor mounted on wheels for odometry was presented in (Coulter et al., 2011) for all kinds of wheelchairs. In (Sonenblum et al., 2012), this sensor was validated for the measurement of wheelchair movement as a tool for clinical experiments in the area of shoulder health and to collect data for wheelchair improvements. The sensor is mounted on the wheel as in Figure 1 and the wheel angle is derived from low-pass filtered a_1 and a_2 accelerometers using $atan2$. The result is again low pass filtered using a butterworth characteristic with a 3 Hz cut off selected to fit the maximal wheelchair speed of 1.5 m/s (downhill) and then doubled. Based on MEMS sensors, it records the data on an SD-card for offline analysis. The description of hard and software for this sensor is available in (Sonenblum, 2010). The method inherently produces angle errors while the wheelchair is accelerated or exposed to noise from driving over uneven terrain. However, this method is acceptable for hand operated wheelchairs, since the acceleration of such vehicles is very limited, and large wheels rotate slowly and suppress noise from uneven terrain better than small wheels.

In (Huang and Wang, 2011), a similar sensor was developed for an inertial measurement system used on bicycles by fusing odometry with a compass as a support for a GPS-based navigation system. The sensor uses two accelerometers (no gyroscope) and transmits the data via Bluetooth to an Android based smartphone. They use a very similar approach of low pass filters and $atan2$ angle computation as in (Sonenblum et al., 2012). Due to the increased wheel rotational speed, they observed significant acceleration shifts on the a_2 accelerometer, and also on the a_1 accelerometer (e.g. when the bicycle brakes). To cope with centrifugal force, accelerometers were configured to the maximal available range of 8 g. Offsets from growing centrifugal forces (a_2) or vehicle acceleration (a_1) were computed by low pass filtering the corresponding signal to subtract them from the original signal before angle computation.

All these approaches address the sensor-fusion problem in a rather heuristic way. Our contribution here is to provide a principled textbook-style solution that *a*) identifies how the measurements depend on the wheel motion as the quantity to be estimated and *b*) uses an Extended Kalman Filter to do the sensor fusion based on the model obtained in *a*).

3 SENSOR HARDWARE

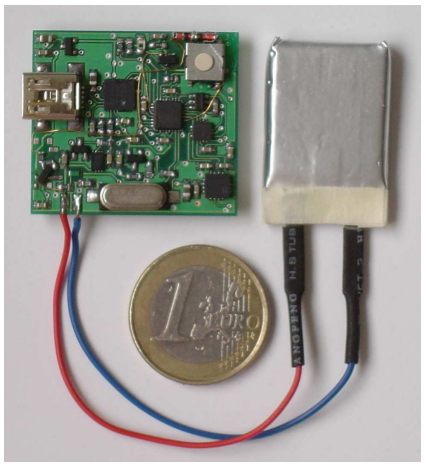

Figure 2: Prototype sensor with 3 axis accelerometer and 3-axis gyroscope used as a wheel sensor on a walker (see Figure 3).

The experiments were conducted using two different sensors. The prototype sensor in Figure 2, which was mounted on a walker wheel shown in Figure 3, uses MEMS sensors from STMicroelectronics, a 3-axis accelerometer (MMA7361L), a 2-axis gyroscope (LPR530AL), and a single gyroscope (LY530ALH). Raw sensor data is sent out via Bluetooth Serial Port

Profile (SSP) at a (low) frequency of $\sim 40\ Hz$, and time stamped later in the receiving PC. According to the datasheets, the limits are 6 g ($g = 9.81\ m/s^2$) and 1200 deg/s (20.9 rad/s), and the board reaches 4.8 g and 8.2 rad/s. Mounted on a small hard plastic wheel with radius $r_w = 10\ cm$ and the sensor chip at a radius of about $r_s = 7\ cm$ (instead of a more centered position for reduced centrifugal force), the conditions for producing good results are not ideal. Although the noise level is high, it is still small compared to noise produced by driving on uneven terrain, and could therefore be used for the experiments.

Figure 3: Prototype sensor mounted on a light-weight walker standing on cobblestone with wireless data communication.

The second sensor is a standard smartphone (Samsung Galaxy S2), mounted on a bicycle wheel hub as shown in Figure 4 and used as a data recorder for offline analysis. According to (Chipworks, 2011), it contains MEMS sensors from STMicroelectronics, a 3-axis accelerometer (LIS3DH) with limits configurable between 2 and 16 g, and a 3-axis gyroscope (L3G4200D) configurable with 250, 500, or 2000 deg/s, but the Android API can only use the default configuration of 500 deg/s and 2 g. Sensor data is received time stamped through the API at a rate of ~ 70 Hz. It is used here to show a reference recording under optimal conditions, and for a long distance test (Section 5.4).

4 EKF BASED SENSOR FUSION

4.1 Overview of the Extended Kalman Filter

The Extended Kalman Filter (EKF) is a generic sensor fusion algorithm for non-linear state estimation. A very accessible introduction is given by (Welch and Bishop, 1995) and we refer the reader to Table 2.1 and 2.2 therein for the concrete equations.

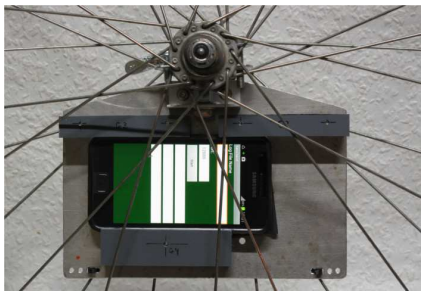

Figure 4: A Samsung Galaxy S2 as a wheel sensor at radius $r_s = 9.5\ cm$ in a bicycle wheel of radius $r_w = 35\ cm$ for data logging.

Conceptually, the EKF computes an estimate $\hat{x}_k$ for an unknown state vector x_k at every point in time k from a sequence of measurement vectors $z_{1\ldots k}$ providing noisy information about the state x_k and optionally control inputs $u_{1\ldots k}$ which we don't need here. The point that makes the EKF attractive is that it updates recursively an internal state representation with each arriving z_k (and u_k).

This computation is based an a) a process model f that maps a former state (optionally control input), and noise values to a new state thereby describing, how the state changes over time and b) a measurement model h that maps state and noise values to a measurement.

In our implementation of wheel odometry with an EKF, the generic filter algorithm is provided by the kfilter-library from (Zalzal, 2013), while the specific process and measurement model are developed in the following subsections.

4.2 State Representation

For wheel odometry the desired quantity is the position p, i.e. the travelled horizontal distance of the vehicle (measured at the center of the wheel, not at the sensor). We drop the index $_k$ here for simplicity. As we assume a non-slipping wheel, the wheel angle θ relates linear to p as

$$\theta = \frac{p}{r_w} \tag{1}$$

with wheel radius r_w. The sensor itself however, makes a spiralling motion composed of a translation by p and a rotation by θ. This complex motion leads to the following effects (Huang and Wang, 2011) observed through the sensor (Figure 1):

The gyroscope ω observes

1. Rotation, i.e. $\dot{p}$;
2. Sensor noise.

The accelerometers a_1, a_2 observe

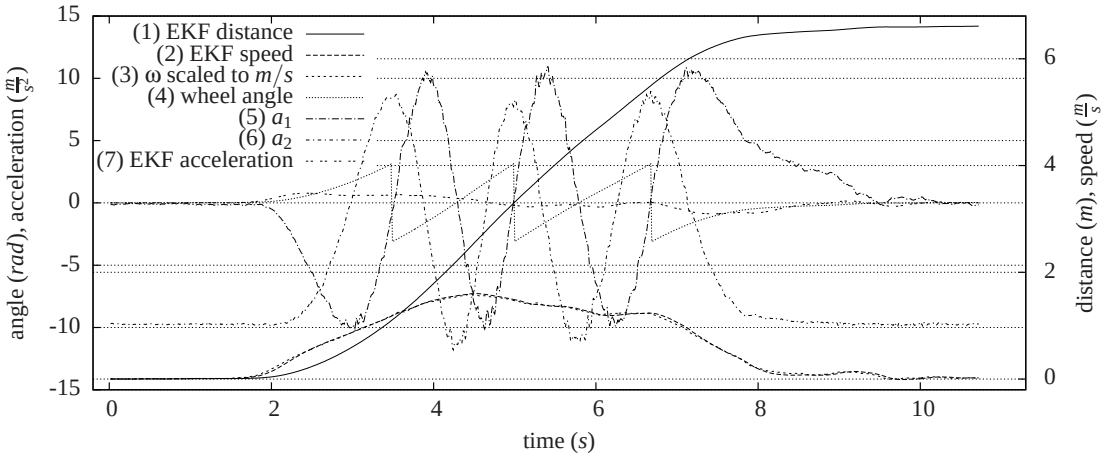

Figure 5: Measurement using the Galaxy S2 sensor (Figure 4) in a bicycle wheel shuffled indoor over a distance of 6.6 *m* at walking speed.

3. Gravity;
4. Vehicle acceleration $\ddot{p}$;
5. Angular acceleration in a_1, which is proportional to $\ddot{p}$
6. Centrifugal acceleration in a_2, which is proportional to $\dot{p}^2$;
7. Acceleration caused by uneven terrain;
8. Sensor noise.

We model the last two items as white noise. To model the other effects as a function f of the state x, the state x consists of

$$x = \begin{pmatrix} p \\ \dot{p} \\ \ddot{p} \end{pmatrix} \tag{2}$$

i.e. position, velocity and acceleration.

It is common practice to include only position and velocity in the state and model the accelerometer measurement as change in velocity in the control input u (similar with the gyroscope). This is difficult here, as from the above list of effects the relation between measured acceleration and the state is rather complex, so we chose also to include the acceleration $\ddot{p}$ in the state.

4.3 Process Model

As usual, the process model $x_{k+1} = f(x_k, w_k)$ simply integrates $\ddot{p}$ twice for a duration of Δt starting from $\dot{p}$ and p. It assumes that white noise added to the acceleration (resulting implicitly also velocity and position noise).

$$f\left(\begin{pmatrix} p \\ \dot{p} \\ \ddot{p} \end{pmatrix}, w\right) = \begin{pmatrix} p & + & \dot{p}\Delta t & + & \frac{1}{2}\ddot{p}\Delta t^2 \\ & & \dot{p} & + & \ddot{p}\Delta t \\ & & & & \ddot{p} \quad +w \end{pmatrix} \tag{3}$$

The acceleration is modeled as a so-called random walk, i.e. accumulated small random noise, which means that the acceleration may change smoothly over time. As usual, the noise value w is unknown, assumed zero mean, independent and with known variance $q = (0.07\ m/s)^2$. In addition, equation (3) defines that noise occurs only by this uncertain acceleration, since in principle every change in position is caused by velocity and every change in velocity is caused by acceleration.

4.4 Measurement Model

As the process model is completely driven by the state, there is no control input u, both the accelerometers and gyroscope are modeled as measurements z. The measurement $z = (a_1, a_2, \omega)^T$ consists of the two accelerometer measurements a_1, a_2 and the gyroscope measurement ω (Figure 1).

The measurement model $z_k = h(x_k, v_k)$ formalizes the items from Section 4.2, defining how the measurement z depends on the state x and the noise values v (all at time k):

$$h\left(\begin{pmatrix} p \\ \dot{p} \\ \ddot{p} \end{pmatrix}, \begin{pmatrix} v_1 \\ v_2 \\ v_3 \end{pmatrix}\right) = \begin{pmatrix} -g\sin\theta & + & \ddot{p}\cos\theta & - & \ddot{p}\frac{r_s}{r_w} & + & v_1 \\ -g\cos\theta & - & \ddot{p}\sin\theta & - & \dot{p}^2\frac{r_s}{r_w^2} & + & v_2 \\ & & & - & \dot{p}\frac{1}{r_w} & + & v_3 \end{pmatrix} \tag{4}$$

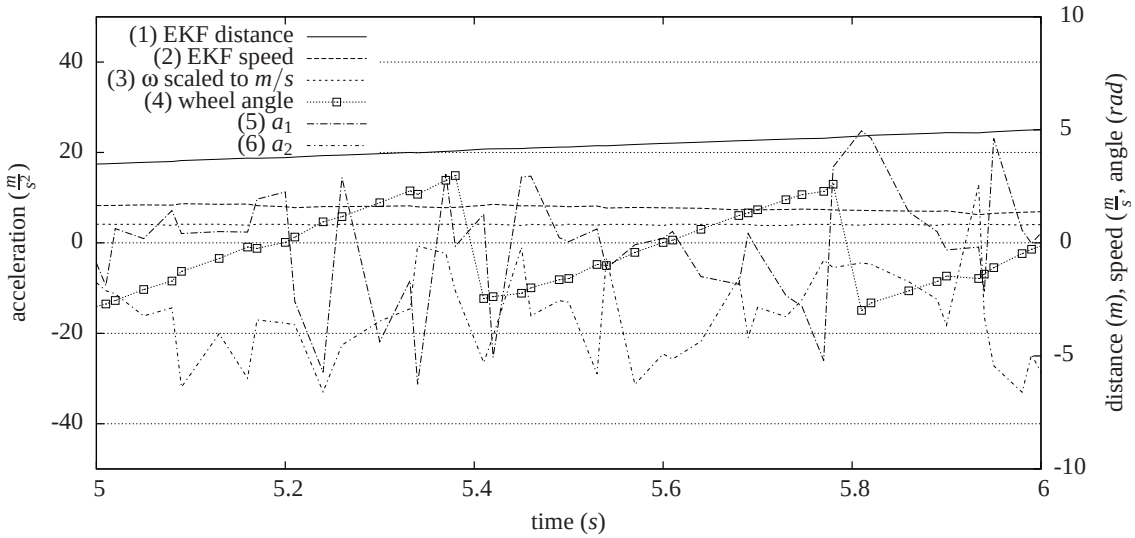

Figure 6: The sensor of figure 2 at radius $r_s = 7\ cm$ on a walker with a wheel radius of $r_w = 10\ cm$. It shows 1 second with about 2.5 wheel revolutions while driving at an extremely uncomfortable speed of 1.5 m/s on cobblestone near the limit of the EKF filter.

where $\theta = \frac{p}{r_w}$, r_s is the radius of the sensor placement on the wheel (Figure 1) and $\theta = 0$ corresponds to the sensor in lowest position. Equation 4 models gravity (1st column), translational acceleration (2nd column), and angular as well as centrifugal acceleration (3rd column) in the first two rows for the accelerometer measurements a_1 and a_2. Gravity and translational acceleration include sine and cosine terms because their direction is world-fixed but measured by a rotating sensor. On the contrary, angular and centrifugal acceleration are sensor fixed as they "rotate with the sensor".

The third row simply models the rotational velocity $\dot{\theta}$ of the wheel as measured by the gyroscope.

All three measurements are perturbed by white Gaussian noise $v_{1...3}$, which is as usual unknown and assumed independent with zero mean and variance $r_{1,2} = (5\ m/s^2)^2$ for the accelerometer and $r_3 = (0.5\ rad/s)^2$ for the gyroscope. The large accelerometer noise models uneven terrain.

As noted in Section 3, the gyroscopes of both sensors do not measure rotation speeds above 10 rad/s. Therefore, a dynamic variance increased to $r_3 = (150\ rad/s)^2$ was used, when the gyroscope was operated in saturation. Increasing and decreasing the variance for r_3 smoothly increases the stability of the filter.

Larger centrifugal forces can also lead to a saturation of the a_2 accelerometer (see Section 5.2). Fortunately, the filter continues to work under these conditions, benefitting from using a dynamic variance increased to $r_2 = (1200 m/s^2)^2$ for the a_2 measurement to (almost) ignore this value. The variance r_2 is also smoothly increased and reduced as for the gyroscope.

4.5 Intuitive Understanding

In this section we provide an intuitive answer to the question *Where does the distance information p come from?*

In slow motion a_1 and a_2 effectively measure gravity only, i.e. $\sin\theta$ and $\cos\theta$, while the gyroscope measures $\dot{\theta}$. Therefore, the overall EKF fuses rather precise differential information (gyroscope) with rather imprecise absolute information (accelerometers). Such a scenario is very common, for instance in robot localization (Thrun et al., 2005).

With faster and more unsteady motion the situation is more difficult, as heavy accelerations strongly perturb (a_1, a_2) in one dimension. However, as long as the gyroscope is still working the filter only needs some average information over roughly a revolution to prevent the gyroscope errors from accumulating. This information is available, since the integral of $\ddot{p}$ is proportional to the velocity measured by the gyroscope.

It is more surprising that the filter still works in fast motion and without a gyroscope (due to saturation), as we will report in section 5.2. To our judgement, at higher speeds the gravity acceleration has a very periodic pattern on which the filter "locks in", similar to a PLL (phase-locked loop) radio receiver.

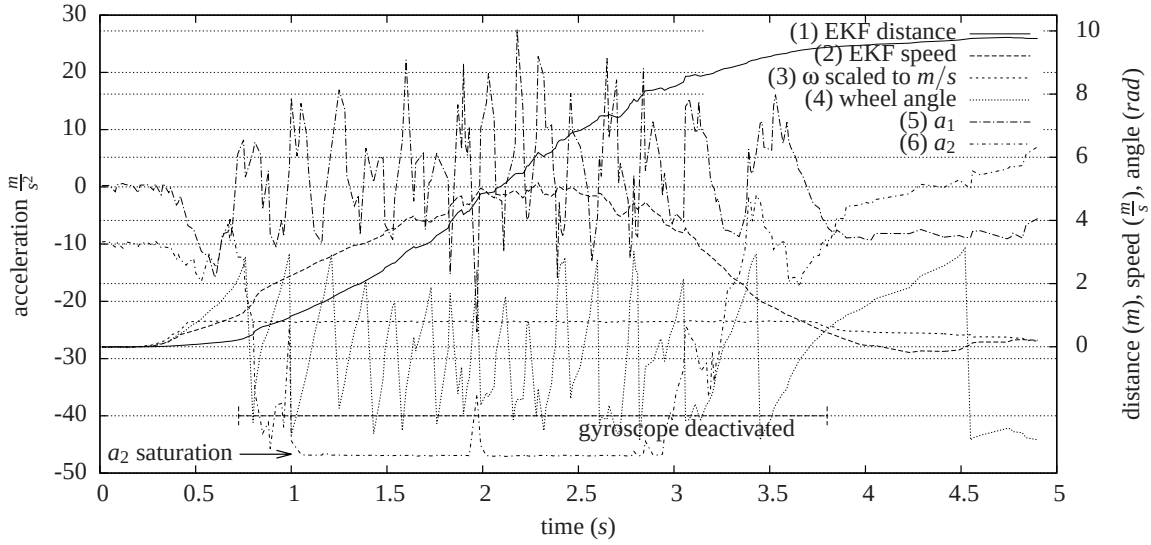

Figure 7: Measurement using the configuration from Figure 6 driving indoor on a carpet. The walker was accelerated and stopped on a distance of 9.70 m to a maximum speed of about 4 m/s.

5 MEASUREMENTS AND RESULTS

The filter has been implemented as a standalone C++ program using the kfilter-library from (Zalzal, 2013) for offline optimizations, and as a real time application in SimRobot, a C++ framework for robotic applications (Laue and Röfer, 2008).

It has been tested with different hardware under normal conditions, as well as under extreme conditions to show its limits. For the intended application area, the focus is to demonstrate the correct recognition of complete wheel revolutions. Therefore, the rolling distance for each experiment was measured to check the deviations of the sensor measurement, and the obtained graphical representation was double checked to identify the combination of missing or false detection of wheel revolutions. The long distance test described in Section 5.4 uses an independent sensor to count wheel revolutions.

Figure 5 shows a measurement using a bicycle wheel with the Samsung Galaxy S2 shown in Figure 4 under optimal conditions and walking speed. The travelled distance measured by the EKF is shown by curve (1), the EKF speed (2) and the gyroscope measurement (3) are almost identical (the curve at the bottom). The rotational speed of the gyroscope was scaled to its corresponding vehicle speed to allow a comparison with the derived EKF speed. The wheel angle (4) is derived from the EKF distance (normalized to a range from $-\pi$ to π) for the interpretation of the sensor inputs a_1 (5) and a_2 (6), that must be sychronous, if the filter works correct.

5.1 Uneven Terrain

The measurement of Figure 6 was taken from the third in a series of 3 successive measurements with increasing speed, using the lightweight walker driving on cobblestone (Figure 3) and the prototype sensor (Figure 2). The walker reached a speed of 1.5 m/s^2, which is already a very uncomfortable speed. The same speed is mentioned in (Coulter et al., 2011) as the maximal measured speed typically reached by wheelchair drivers using hand propulsion. The hard plastic wheels provide almost no damping and the a_2 measurement contains peaks ranging from $+15$ to -40 m/s^2, which makes it even hard for a human reader to see the sinusodial effect of gravity. The gyroscope was deactivated after 2 seconds (saturation) and activated short before the target.

This experiment shows, that the filter can cope with uneven terrain at a speed near the limit reachable by elderly people, but certainly far beyond a level of comfortable driving, even with a deactivated gyroscope. The observable noise on the EKF distance is significant, but would be much smaller using a gyroscope covering the full measurement range, as discussed in Section 5.3.

5.2 High Speed

Figure 7 uses the walker from Section 5.1 for driving in an indoor environment on a carpet over a dis-

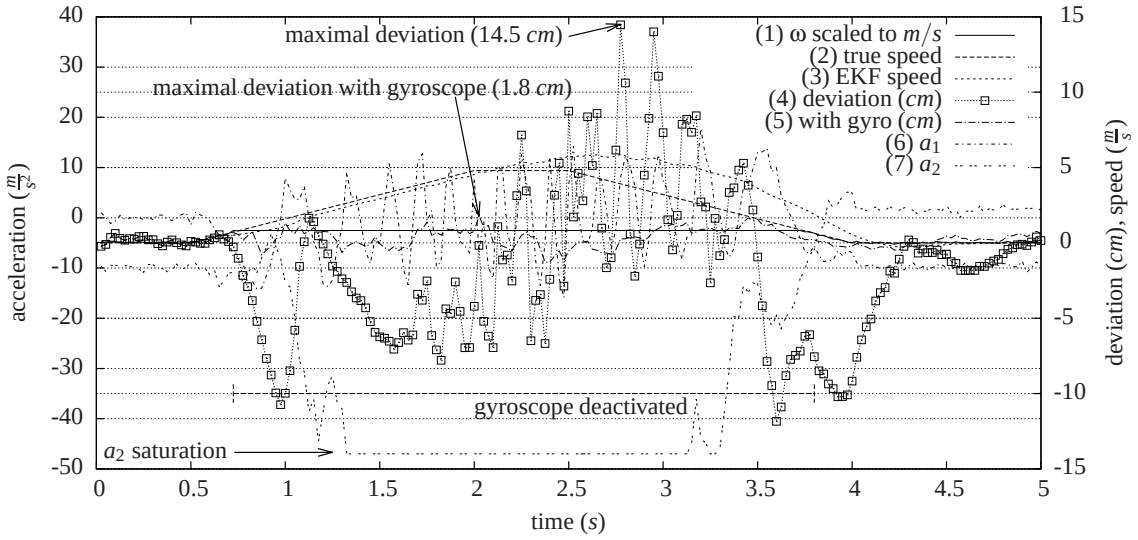

Figure 8: Simulated scenario based on the measured data of the scenario in Figure 7. The simulation allows the printing of the deviation between EKF distance and true distance (4).

tance of 9.70 *m*. The walker was accelerated (shuffled) within 2 seconds to a maximum speed above 4 m/s. The gyroscope is saturated after 0.7 *s*. Centrifugal force reaches values of about 12 *g* in this experiment, which saturates the a_2 accelerometer (6) after one second. Again, the EKF derived final distance (1) coincides with the reference measurement.

This experiment is a clear indication, that our EKF filter can cope with high speeds and heavy accelerations, even if two of the three sensors are already in saturation. The reached speed is far beyond the speed reachable by users dependent on a walker.

5.3 Angle Truth

Comparing the computed angle with the real angle is desirable, but requires an independent secondary odometry sensor, which may introduce additional uncertainties, especially considering synchronization. To analyse the EKF filter alone, we place it in a simulation loop based on the kinematic model used for the filter itself, and feed the filter with (noisy) sensor input based on a fully known state *x*.

Figure 8 is a simulation of the high speed scenario described in Section 5.2. Here, the difference between simulated position and the derived distance is given as the dotted line (4) in *cm*. In this scenario, the vehicle was accelerated for 1.5 *s* with 3.2 m/s^2, rolled for 0.5 *s*, and then braked with -3.2 m/s^2, the resulting simulated speed is visualized as curve (2). The sensor data contains noise using a normal distribution (Box and Muller, 1958) with a standard deviation $\sigma = (0.5 + \dot{p})\ m/s^2$ for the accelerometers (curve (6) and (7)). The noise grew with the simulated speed to create noise similar to noise from driving on uneven terrain. For the gyroscope, $\sigma = 0.5\ m/s$ and a linear error by multiplication with 1.01 were chosen. The maximal difference of 14.5 *cm* (wheel angle error near 90 degrees) confirms this example to be an extreme case. Although speed and acceleration where chosen extremly high, the EKF filter did not loose a single wheel revolution.

This experiment was repeated with the gyroscope measuring the full range of angular speed (no gyroscope saturation). Curve (5) in Figure 8 is the difference for this configuration, where the maximal deviation does not exceed 1.8 *cm*.

In this example, while driving over a distance of 9.70 *m*, the gyroscope would overestimate the distance due to its linear error by nearly 10 *cm*. The filter corrects the gyroscope measurement using the additional information from the a_1 accelerometer to correct this error, reducing it to an overall maximal difference of 1.8 *cm*. Using the gyroscope not only increases the precision, it also suppresses underground noise as it is mainly unaffected by vibrations.

5.4 Long Distance

For a long distance test, the bicycle sensor was used over a distance of 4 km in an urban environment with segments of cobblestone and typical bumps at speeds up to 6 m/s (22 km/h). As a reference measurement, a magnet was attached to the fork carrying the wheel to count complete wheel revolutions. The result was 1828 wheel revolutions for the magnetic

counter, 1827.6 for the EKF filter. It therefore works correctly in a practical scenario.

6 CONCLUSIONS

This paper presents a sensor fusion algorithm for a wheel mounted accelerometer and gyroscope based odometry sensor. In contrast to existing approaches using ad hoc methods to derive wheel angles, the presented solution uses an Extended Kalman filter as a principled estimator for locally linear systems observed by noisy sensors. The power of this algorithm is demonstrated by the overall positve results of a number of experiments using real hardware under normal as well as extreme conditions, and by simulation experiments to compare the filter output against a well known true state. The filter adapts dynamically to saturation of the gyroscope and of the centrifugal force accelerometer at high speed and continues to work with even a single accelerometer. Embedded in a small hardware component, it will provide a very simple way of belated or temporary installation for existing vehicles.

ACKNOWLEDGEMENTS

The author wishes to thank Hui Shi for her intensive rereading, Christian Mandel and Christoph Budelman for providing the prototype sensor, and Bernd Krieg-Brückner as the initiator for this work and coordinator of the (collaborative) project ASSAM (EU AAL Joint Programme AAL-2011-4-062, Call 4 *ICT Based Solutions for Advancement of Older Persons' Mobility*.

REFERENCES

Bluetooth (2013). Bluetooth Specification Version 4.0. http://www.bluetooth.org/.

Box, G. E. P. and Muller, M. E. (1958). A note on the generation of random normal deviates. *The Annals of Mathematical Statistics*, 29(2):610–611.

Chipworks (2011). Silicon Summary in the Samsung Galaxy S II. http://www.chipworks.com/.

Coulter, E. H., Dall, P. M., Rochester, L., Hasler, J. P., and Granat, M. H. (2011). Development and validation of a physical activity monitor for use on a wheelchair. *Spinal Cord 2010*, 49:455–50.

Huang, J.-D. and Wang, T.-W. (2011). Accelerometer based wireless wheel rotating sensor for navigation usage. In *Sensing Technology (ICST), 2011 Fifth International Conference on Sensing Technology*, pages 565–568.

Kalman, R. E. (1960). A new approach to linear filtering and prediction problems. *Transactions of the ASME–Journal of Basic Engineering*, 82(Series D):35–45.

Krieg-Brückner, B., Bothmer, H., Budelmann, C., Crombie, D., Guerin, A., Heindorf, A., Lifante, J., Martinez, A., S.Millet, and Vellemann, E. (2012). Assistance for Safe Mobility: the ASSAM Project. In *Proceedings of the AAL-Forum 2012*, Eindhoven.

Krieg-Brückner, B., Gersdorf, B., Mandel, C., and Schröder, M.-S. (2013). Navigation Aid for Mobility Assistants. In *Proceedings of the Joint CEWIT-TZI-acatech Workshop "ICT meets Medicine and Health" ICTMH 2013*.

Laue, T. and Röfer, T. (2008). SimRobot - Development and Applications. In *Proceedings of the International Conference on Simulation, Modeling and Programming for Autonomous Robots SIMPAR 2008*.

OpenStreetMap (2013). OpenStreetMap - The Map. http://www.openstreetmap.org/.

Sonenblum, S. (2010). How to Build a Wheelchair Data Logging System. http://www.mobilityrerc.gatech.edu/wheelchair_data_ logger.php/.

Sonenblum, S. E., Sprigle, S., Caspall, J., and Lopez, R. (2012). Validation of an accelerometer-based method to measure the use of manual wheelchairs. *Medical Engineering Physics*, 34(6):781–786.

Thrun, S., Burgard, W., and Fox, D. (2005). *Probabilistic Robotics (Intelligent Robotics and Autonomous Agents)*. The MIT Press.

Welch, G. and Bishop, G. (1995). An introduction to the Kalman filter. Technical Report 95-041, University of North Carolina, Chapel Hill, NC, USA.

Zalzal, V. (2013). KFilter - Free C++ Extended Kalman Filter Library. http://http://kalman.sourceforge.net/.